Nanocomposites of Poly(vinylidene fluoride) with Multiwalled Carbon Nanotubes

Wenwen Huang,[1] Kyle Edenzon,[2] Luis Fernandez,[3] Shabnam Razmpour,[2] Jenna Woodburn,[4] Peggy Cebe[1]

[1]*Tufts University, Department of Physics and Astronomy, Medford, Massachusetts 02155*
[2]*Rochester Institute of Technology, Department of Biological Sciences, Rochester, New York 14623*
[3]*Rochester Institute of Technology, Department of Science and Mathematics, Rochester, New York 14623*
[4]*Gallaudet University, Department of Chemistry and Physics, Washington, District of Columbia 20002*

Received 30 April 2009; accepted 4 September 2009
DOI 10.1002/app.31393
Published online 3 November 2009 in Wiley InterScience (www.interscience.wiley.com).

ABSTRACT: The preparation and characterization of nanocomposites of poly(vinylidene fluoride), PVDF, with acid treated multiwalled carbon nanotubes (MWCNT) with a wide composition range, from 0.1 to 5.0% MWCNT by weight, is reported. Effect of uniaxial orientation by zone drawing on these nanocomposites is discussed and compared with unoriented compression molded films. Static room temperature two-dimensional wide angle X-ray scattering and Fourier transform infrared spectroscopy were used for phase identification. Differential scanning calorimetry, polarizing optical microscopy, dynamic mechanical analysis (DMA), and thermogravimetic analysis (TGA) were used to study the thermal and mechanical properties. Incorporation of MWCNT into PVDF has no obvious effect in forming beta phase crystal in the PVDF/MWCNT bulk films, while zone drawing cause a significant alpha to beta transition in PVDF/MWCNT. Results indicate that MWCNTs act as nucleation agent during crystallization and slightly increase the degree of crystallinity of PVDF/MWCNT bulk films. TGA indicates the thermal stability is improved when MWCNT concentration increases for unoriented PVDF/MWCNT film. The modulus also increases significantly when MWCNT concentration increases. The glass transition temperature measured by the peak position of tanδ from DMA does not change with MWCNT concentration, but a slightly higher glass transition can be obtained by zone drawing. J Appl Polym Sci 115: 3238–3248, 2010

Key words: poly(vinylidene fluoride); PVDF; multiwalled carbon nanotubes; MWCNT; nanocomposites; uniaxial orientation; zone drawing

INTRODUCTION

Poly(vinylidene fluoride) (PVDF) is one of the most important thermoplastics used in a variety of modern engineering application such as in sensors, actuators, and energy transducers.[1] A wide range of studies of PVDF have been reported due to its good mechanical properties, and attractive piezoelectric and pyroelectric properties.[1–9] PVDF crystallizes into five crystallographic forms. The two major forms of interest of our present work are: the polar *tttt* beta phase (form I) and the nonpolar tg^+tg^- alpha phase (form II).[2,3]

In 1969, Kawai first discovered the piezoelectric property in PVDF.[4] Shortly after that, in 1971, pyoelectric property was discovered in PVDF by Bergman et al.[5] Their studies show when stressed or under changes in temperature, PVDF undergoes a change in electric polarization. The beta PVDF crystal is polarized and transduces electric energy into motion (or vice versa), thus is technologically preferred, while the alpha PVDF crystal does not. Normally alpha PVDF crystal is more easily obtained. To obtain the beta PVDF crystal, special treatments are commonly used: (1) uniaxial mechanical drawing alpha PVDF film at temperature between 80 and 140°C,[6] (2) crystallizing from *N,N*-dimethylformamide (DMF) or *N,N*-dimethylacetamide (DMAc) solutions below 70°C,[7] and (3) modifying the polymer with nanoparticle addition.[8,9] Using method 1, one can seldom get complete alpha-beta conversion. Approximately 20% of alpha PVDF will remain, depending on the drawing temperature. Method 2 can form almost exclusively beta PVDF film, but the film is brittle and with high degree of porosity. Method 3 was the most intensively studied one, not only because it can form almost exclusively beta phase PVDF film, but also it can improve the thermal and mechanical properties of the polymer. For PVDF nanocomposite with more than 0.5 wt % organically modifies silicate clay, the beta phase dominates, and the glass transition temperature and

Correspondence to: P. Cebe (peggy.cebe@tufts.edu).
Contract grant sponsor: National Science Foundation; contract grant number: DMR-0704056.

storage modulus are also higher than in the homopolymer.[9]

Ever since the discovery of carbon nanotubes (CNTs) by Iijima in 1991,[10] the use of CNTs as a nano-filler for polymers, such as polystyrene, poly(vinylidene fluoride), poly(methyl methacrylate), polycaprolactam (nylon-6), and isotactic poly(propylene), has been receiving increasing attention.[11–15] Two forms of CNTs exist: single-walled carbon nanotubes (SWCNTs) and multiwalled carbon nanotubes (MWCNTs). SWCNTs comprise a single sheet of graphite rolled into a cylinder; multiwalled carbon nanotubes (MWCNT) consist of concentric cylinders around a hollow center with constant wall to wall separation of 0.34 nm.[16] The Young's modulus of MWCNT is about 1.8 TPa,[17] and appears to be a function of the number of walls, as reported by both theoretical and experimental works.[16,18] The thermal conductivity of MWCNT can be more than 3000 W/m-K.[19] By dispersing MWCNT into polymer matrix, it is expected that polymer properties can be enhanced with a higher thermal conductivity, higher electrical conductivity, and large Young's modulus. Another advantage for MWCNT use as a nano-filler is its large surface area and high aspect ratio, which induce a better adhesion of polymer. However, despite the attractive properties mentioned above, using CNTs as nanofillers has its own draw back in producing polymer nanotube composites: dispersing the nanotubes uniformly into the polymer matrix is difficult due to the Van der Waal's force existing in between the carbon nanotubes, and due to their small size. Several methods have been studied to overcome this problem, including chemical modification of the surface of CNTs, grafting polymer on to CNTs, solution method, and direct mixing in melt processing.[20]

In our present work, we report a characterization study of PVDF/MWCNT films prepared from solution over a wide composition range, from 0.1 to 5.0% MWCNT by weight. The MWCNT was purified by acid treatment. Effect of uniaxial orientation by zone drawing on these nanocomposites is also discussed and compared with unoriented compression molded films. The purpose of this study is to determine separate effects of uniaxial drawing and the MWCNT modification of PVDF on the phase transition from alpha phase to beta phase in PVDF, and their effect on the thermal and mechanical properties of the PVDF/MWCNT films.

EXPERIMENTAL SECTION

Sample preparation

PVDF used in our present study was a KYNAR® poly(vinylidene fluoride) resin grade 740 commercially obtained from ATOFINA Chemicals, in pellet form. MWCNTs were purchased from MER Corporation with a nominal diameter about 140 nm and length ranging from 5 to 9 μm. To purify the MWCNTs, they were suspended in a mixture of concentrated sulfuric acid and nitric acid (3 : 1 vol ratio) and ultra-sonicated in a water bath for several hours, then washed with deionized water and filtered through a 400 nm pore PTFE membrane until the water passing through the filter had a pH between 6 and 7. After this treatment, the MWCNTs had been functionalized and reach a purity of 95%.[21]

To achieve uniformly mixed PVDF/MWCNT solutions with desired weight percentages of MWCNT, a two step method was used. First, two stock solutions were prepared: PVDF was dissolved and MWCNTs were separately dispersed in dimethylacetamide (DMAc) solution with stirring for about 3 days at 30–40°C. Then, two stock solutions were mixed to achieve the desired weight percentages of MWCNTs from 0.1 to 5%. The PVDF/MWCNT solutions were stirred for 2 days at 30–40°C and then ultra-sonicated in water bath for 10 min. To remove the DMAc solvent, PVDF/MWCNT solutions were poured into uncovered preheated glass Petri dishes and uniformly heated at 60°C for 1 day. Curly films formed after evaporation of DMAc, and could be easily lifted from the glass Petri dishes. Because MWCNTs are black in color, the films containing more MWCNTs look darker: film colors varied from tan (0% MWCNT) to light gray (1% MWCNT) to dark black (5% MWCNT). Uniform color was observed, an indication of good distribution (i.e., little or no large scale aggregation) of MWCNTs in the polymer matrix. To achieve flat bulk films, about 100 micrometers thick, all compositions were compression molded using a Carver hydraulic hot press at a pressure of 12 MPa, at 200°C for 3 min, well above the melting point of PVDF (178°C) and then were air cooled. Figure 1 shows a scanning electron microscope (SEM) image of MWCNTs after purification and evaporation of DMAc, which showed that those treatments did not change the morphology of MWCNTs compared to the untreated MWCNTs (not shown for the sake of brevity).

Zone drawing experiments[22,23] were performed at a fixed temperature, 105°C ± 5°C, with an almost constant applied stress, 2.3 kg/m^2. During this process, the samples became oriented so that the crystallographic c-axis and molecular chain axes were partially aligned along the zone drawing direction. The a-axis and b-axis were randomly oriented in the plane perpendicular to the draw direction. The draw ratio, λ, was calculated from:

$$\lambda = L_f/L_i \quad (1)$$

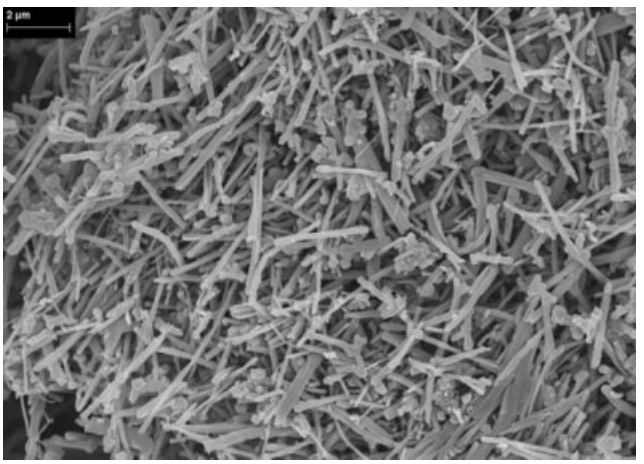

Figure 1 Scanning electron microscope (SEM) image of MWCNT powder after acid treatment and evaporation of DMAc.

where L_f is the final length of the film after drawing and L_i is the initial length of the film. Though there was a large standard error (±12.5%) of the draw ratio for each composition, which may due to non-uniformity of the film thickness, the draw ratio for all the samples we investigated was in the range of 4.7 ± 0.3.

Analysis methods

Room temperature two-dimensional (2D) wide angle X-ray scattering (WAXS) was performed on a Bruker GADDS D8 X-ray diffractometer, with wavelength $\lambda = 0.154$ nm, operated at 40 kV and 20 mA. Scattering angle, 2θ, was calibrated by using silicon powder reference standard with silicon (111) peak at 28.444°, for all the undrawn and drawn films. The scan time used was 600s per sample. The scattering angle, 2θ, ranged from 5° to 30°. The air background was subtracted from the original scan for each sample. To compare the peak position and identify the crystalline content, the 2D WAXS patterns were converted to a one-dimensional pattern by integrating over a sector. The crystallinity index, $\phi_{ci,}$ the fraction of alpha, ϕ_{alpha}, and the fraction of beta phase, ϕ_{beta}, were calculated using the area of crystal peaks and area of amorphous halo by fitting the Lorentz-corrected WAXS peak intensity using Gaussian wavefunctions as described previously.[9]

Room temperature Fourier transform infrared spectroscopy (FTIR) studies were performed using a Jasco FT/IR-6200 with a TGS detector in attenuated total reflection (ATR) mode. The absorbance spectra were obtained by averaging 64 scans with a resolution of 4.0 cm^{-1}. The background spectra were collected under the same conditions and subtracted from the scan for each sample. The wavenumbers investigated ranged from 600 to 4000 cm^{-1}.

Differential scanning calorimetry (DSC) was performed on a TA Instruments 2920 temperature modulated differential scanning calorimeter (TMDSC) in standard mode. The same heating/cooling method was used for all samples: they were heated at a rate of 10°C/min from 50 to 200°C and then cooled at a rate of 10°C/min from 200°C to 50°C. Aluminum sample pans were used to encapsulate the sample. A nitrogen purge gas was used at a flow rate of 50 mL/min. The sample weights were in the range between 7.5 and 12.0 mg.

Thermogravimetic analysis (TGA) was performed on a TA Instruments Q500 thermogravimetic analyzer at a heating rate of 10°C/min from room temperature to 1000°C in a nitrogen gas flow (60.0 mL/min). The initial sample weight was in the range between 7.0 mg and 11.0 mg.

Polarizing optical microscopy (POM) studies were performed on a Nikon eclipse E600 polarized optical microscope with a Linkam THMS600 hotstage. The heating/cooling method used was the same as the method used for DSC studies.

Dynamic mechanical analysis (DMA) studies were performed on a TA Instruments RSA3 dynamic mechanical analyzer using frequency/temperature sweep test at a strain of 0.1%, with four different frequencies, 0.1, 1.0, 10, and 50 Hz. The temperature ranged from −100°C to 30°C with an increase of 3°C per step and a soak time of 45 s per step.

Tensile tests were performed at room temperature on unoriented samples, using an Instron 3366 with a 100N capacity load cell. Crosshead displacement rates of 2 and 10 mm/min were used. Sample specimens were cut into dog bone shapes with a sharp-edged die ASTM-D-638-5-1MP from ODC Tooling and Molds. Each sample type was run at least three times, and average values are reported.

RESULT AND DISCUSSION

Phase identification

The crystal structure of our films was evaluated by static 2D WAXS as shown in Figure 2(a,b) for the unoriented film and oriented zone drawn film, respectively, exemplified by 1.0 wt % MWCNT. As can be seen, the (h00), (0k0), and (hk0) reflections lie on the equator, while the (0kl) reflection is quadrantal for the oriented sample. By the Laue formula, we can conclude that the ab plane is perpendicular to the sample surface and the drawing direction. The crystallographic c axis is along the drawing direction. The zone drawing process orientated the crystals with polymer molecular chain along the fiber axis (draw direction).

To compare the peak positions of each sample, the intensity was integrated from $\chi = 90$ to 270°

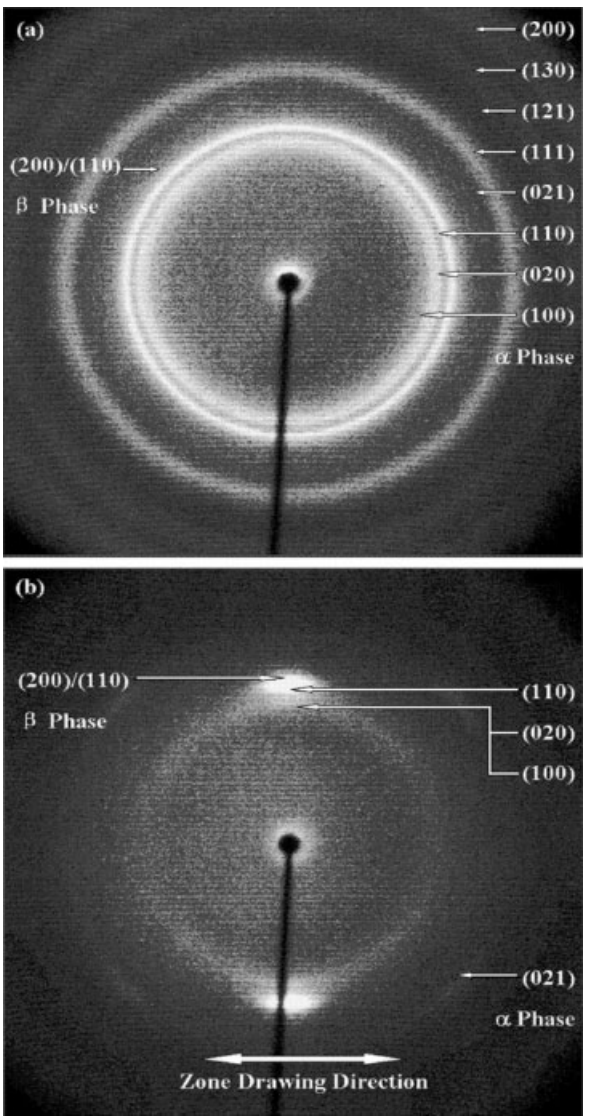

Figure 2 2D WAXS patterns of nanocomposites of PVDF with MWCNT, exemplified by 1.0 wt % MWCNT. (a) Unoriented sample, formed by hot pressing, (b) Oriented sample, formed by hot pressing and then zone drawing. The white arrow at the bottom represents the zone drawing direction. Miller indices for alpha PVDF and beta PVDF are marked.[9]

(the upper half sector) and normalized to 1 by dividing by the greatest intensity for each composition. Figure 3(a,b) compares the 1D WAXS pattern for all unoriented and oriented samples with different MWCNT compositions. For the unoriented PVDF/MWCNT films, Figure 3(a), the major peaks for all compositions were observed at $2\theta = 17.8°$, 18.5°, 20.1°, 26.8°, 28.1°, for $d_{100}(\alpha) = 0.497$ nm, $d_{020}(\alpha) = 0.480$ nm, $d_{110}(\alpha) = 0.443$ nm, $d_{021}(\alpha) = 0.334$ nm, and $d_{111}(\alpha) = 0.318$ nm, respectively.[9] These reflections belong to orthorhombic alpha PVDF which has lattice constants of $a = 0.496$ nm, $b = 0.964$ nm, $c = 0.462$ nm.[24] For films with 0.1 to 5.0 wt % MWCNT, a small shoulder can also be observed at $2\theta = 20.8°$ for $d_{200/110}(\beta) = 0.427$ nm corresponding to pseudo-hexagonal polar beta PVDF crystal which has lattice constants of $a = 0.858$ nm, $b = 0.491$ nm, $c = 0.256$ nm.[3,25] For oriented PVDF/MWCNT films, Figure 3(b), the peak intensity at $2\theta = 20.8°$ increases remarkably while all other peak intensities decrease significantly compared to unoriented samples. This result shows the increase of MWCNTs has no strong effect on forming beta phase crystal for unoriented samples. However, the uniaxial zone drawing process has the very clear effect of transforming alpha phase crystals to beta phase, which has been reported previously.[25] MWCNT did not hinder the alpha to beta crystal transformation in PVDF during zone drawing either.

To estimate the crystallinity index, $\phi_{ci,}$ the fraction of alpha, ϕ_{alpha}, and the fraction of beta phase, ϕ_{beta}, of PVDF/MWCNT films, the Lorentz-corrected WAXS peak intensities were fitted with Gaussian peaks and a quadratic baseline.[9] Figure 4 illustrates the fitting for 1.0 wt % PVDF/MWCNT film. The crystallinity index, $\phi_{ci,}$ was estimated by dividing the area of crystal peaks by the total area of the coherent scattering, which is the sum of the areas of amorphous halo and crystal peaks. This approach has been applied to crystallinity determination in unoriented[9] and oriented samples.[26,27] The fraction of alpha (or beta), ϕ_{alpha} (or ϕ_{beta}), was estimated by dividing the sum of the alpha (or beta) crystal peaks by the total area. The dependence of alpha fraction, beta fraction, and crystallinity index, on MWCNT concentration is shown in Figure 5(a–c), respectively, for all unoriented samples (filled triangles) and oriented samples (open squares). The scattering peak for MWCNT, occurring at $2\theta = 26.29°$ and corresponding to $d_{002} = 0.34$ nm, is neglected due to the small peak intensity.[28,29] We observed from Figure 5 that the beta fraction and crystallinity index increase slightly, and the alpha fraction varies around a constant, with MWCNT addition. This result suggests that MWCNT addition increases crystallinity slightly through enhanced nucleation (POM results show spherulites become smaller with MWCNT addition). On the other hand, MWCNT may also reduce the chain mobility which would hinder the crystallization process. The competition between those two effects of MWCNT makes the trend for crystallinity index hard to predict. From our data, the former one prevails. The maximum beta to alpha ratio, ϕ_{beta}/ϕ_{alpha}, occurred at 1.0 wt % for unoriented films which is in agreement with previous work by Carroll,[12] while the maximum beta to alpha ratio occurred at 2.0 wt % for oriented samples. The decrease of the beta to alpha ratio at higher MWCNT concentration is possibly due to reaggregation within the polymer matrix as the MWCNT concentration increases.[12] We also observed that the

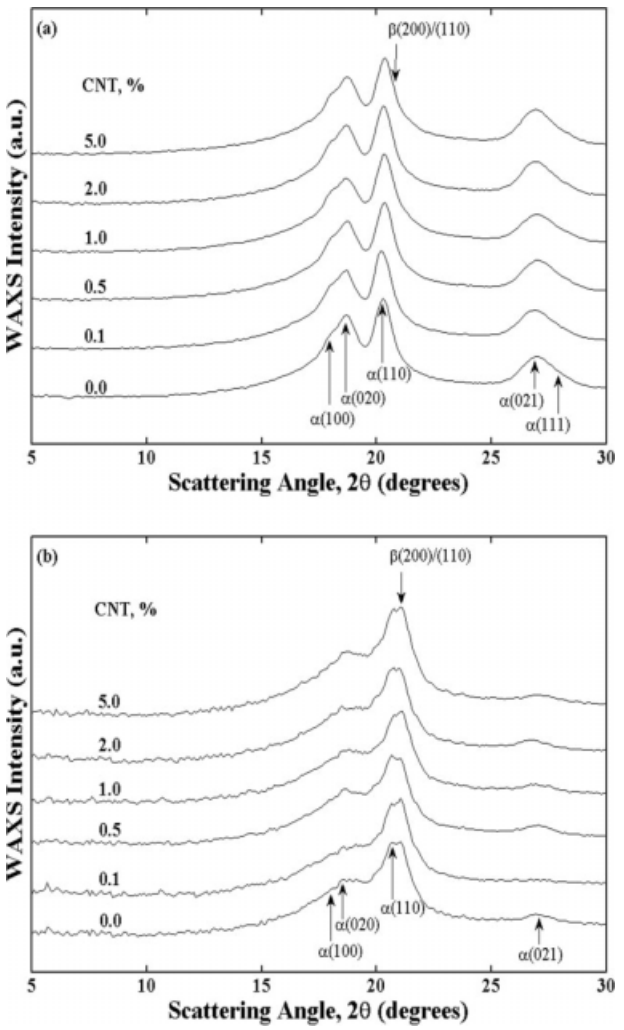

Figure 3 Normalized WAXS Intensity versus scattering angle, 2θ, for nanocomposites of PVDF with MWCNT with composition as indicated. (a) Unoriented samples, (b) Oriented zone drawn samples. Miller indices for alpha and beta PVDF are marked.[9]

alpha fraction and crystallinity index are lower, and beta fraction is higher, for the oriented sample compared to the unoriented sample. This result suggests that the crystalline structure of alpha phase is partially destroyed by the zone drawing process, and all original alpha phase is not completely transformed to beta phase; some was converted to the amorphous phase.

The crystal structure was also investigated by static Fourier transform infrared spectroscopy (FTIR). Figure 6(a,b) shows the FTIR absorbance spectra for unoriented samples and oriented samples, respectively. We observe that the alpha absorption bands at 1383, 976, 764, and 613 cm^{-1}, exist in all compositions. Those peaks correspond to bending and wagging motion of CH_2 (1383 cm^{-1}), twisting motion of CH_2 (976 cm^{-1}), bending motion of CF_2 and skeletal bending of CF—CH—CF (764 cm^{-1}), and bending motion of CF_2 and skeletal bending of CH—CF—CH (613 cm^{-1}).[30] Peaks at 764 cm^{-1} and 613 cm^{-1} were decreased as a function of wt % of MWCNT, which suggest the vibration modes for CF_2 were weakened. This is because hydrogen bonds exist between the carboxyl group on acid treated MWCNT walls and the fluorine atoms in PVDF. A rough estimate of the energy of the O—H...F hydrogen bond is 3 kcal mol^{-1}.[31] Fluorine atoms in PVDF tend to be attracted to MWCNT exterior walls due to this strong hydrogen bond, and the vibrations of CF_2 are thus hindered, which effect was also demonstrated in PVDF nanocomposites with silicates.[32] Whereas in the case of PVDF/silicate nanocomposites there was complete conversion of alpha phase gauche bonds to beta phase all trans,[32]

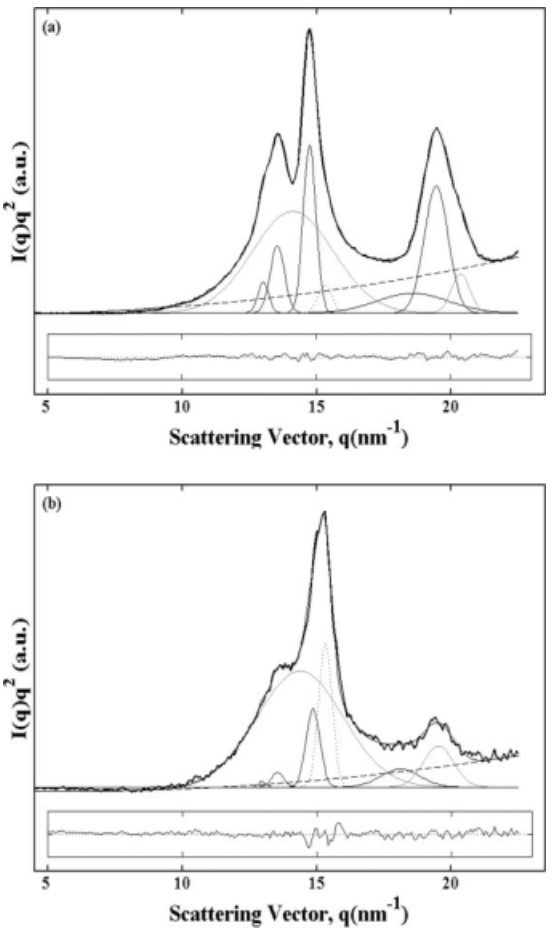

Figure 4 Peak deconvolution of Lorentz-corrected WAXS peak intensity, $I(q)q^2$ versus q, using Gaussian wavefunction and quadratic baseline, for nanocomposites of PVDF with MWCNT exemplified by 1.0 wt %. (a) Unoriented sample, (b) Oriented zone drawn sample. The heavy curve represents the measured data; the gray lines represent the amorphous halos; the solid lines represent the alpha peaks; the dotted lines represent the beta peak; and the dash lines represent the corrected baseline. The insert shows the residual between the fitted curve and measured curve. The dotted line in each insert plot represents the zero position.

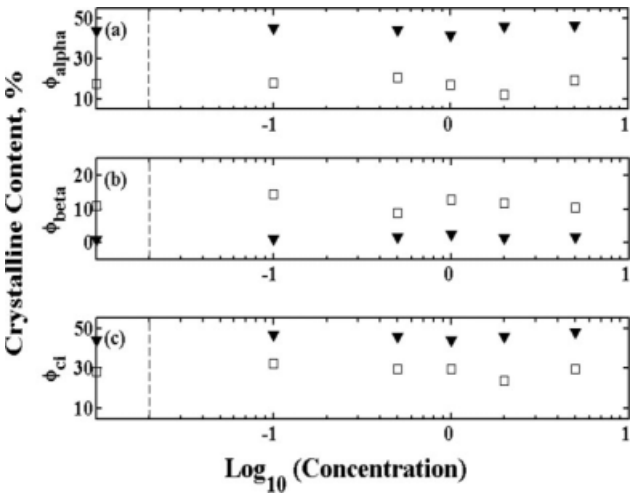

Figure 5 Crystalline content versus MWCNT concentration for nanocomposites of PVDF with MWCNT calculated from Lorentz-corrected WAXS peak intensity fitting analysis, for unoriented samples (black triangles) and oriented samples (white squares). (a) alpha PVDF content, $\phi_{alpha,}$ (b) beta PVDF content, $\phi_{beta,}$ (c) crystalline index, $\phi_{ci} = \phi_{alpha} + \phi_{beta}$. The crystalline content for homopolymer PVDF is marked on the y axis for comparison. The error bar is within each data point.

in our case with MWCNTs, the effect is less, and the beta fraction only increases slightly.

The alpha fraction estimated by FTIR is almost constant. The beta absorption peaks at 1274 and 840 cm^{-1} increased slightly with MWCNT addition and reached a maximum beta fraction at above 1% MWCNT in both cases. These peaks correspond to symmetric stretching motion of CF_2 and CC, and skeletal bending motion of CF—CH—CF (1274 cm^{-1}), and rocking motion of CH_2 and antisymmetric stretching motion of CF_2 (840 cm^{-1}).[30] This result suggests that the MWCNT served as a nucleation agent for beta phase, which cause beta phase to increase slightly in both cases. The zone drawing studies show the beta phase grew at the expense of reducing the alpha phase. This conclusion is consistent with that from 2D WAXS. FTIR absorption peaks for purified MWCNTs are located at 3409, 1708, and 1200 cm^{-1} corresponding, respectively, to OH (3409 cm^{-1}), C=O (1708 cm^{-1}) and C—O (1200 cm^{-1}) stretching in the carboxylic group.[28] These peaks do not overlap with any characteristic peaks for PVDF alpha and beta phase.

Thermal properties

DSC scans of unoriented samples during cooling at 10°C/min from 200°C to 50°C are shown in Figure 7. As MWCNT content increases, the crystallization exothermal extrapolated onset and peak position systematically shift to a higher temperature. The extrapolated onset shifted upward 8°C and the crystallization peak shifted 16°C. This means the sample film with the highest concentration of MWCNTs crystallized first during cooling. DSC scans confirm that the MWCNT acts as nucleation agent. This behavior was also observed by POM studies and is summarized in Table I, column 4.

The degree of crystallinity of PVDF/MWCNT film, χ_c, summarized in Table I column 6, was determined from the area of endotherm peak using:

$$X_c = \Delta H_f / \Delta H_{f(100\%)} \quad (2)$$

where ΔH_f is the measured heat fusion of the PVDF/MWCNT films, and $\Delta H_{f(100\%)} = 104.6$ J/g[3] is the heat fusion of 100% crystalline PVDF. This result is consistent with crystallinity index, $\phi_{ci,}$ from 2D WAXS, showing the crystal portion of the sample will increase with the concentration of MWCNT.

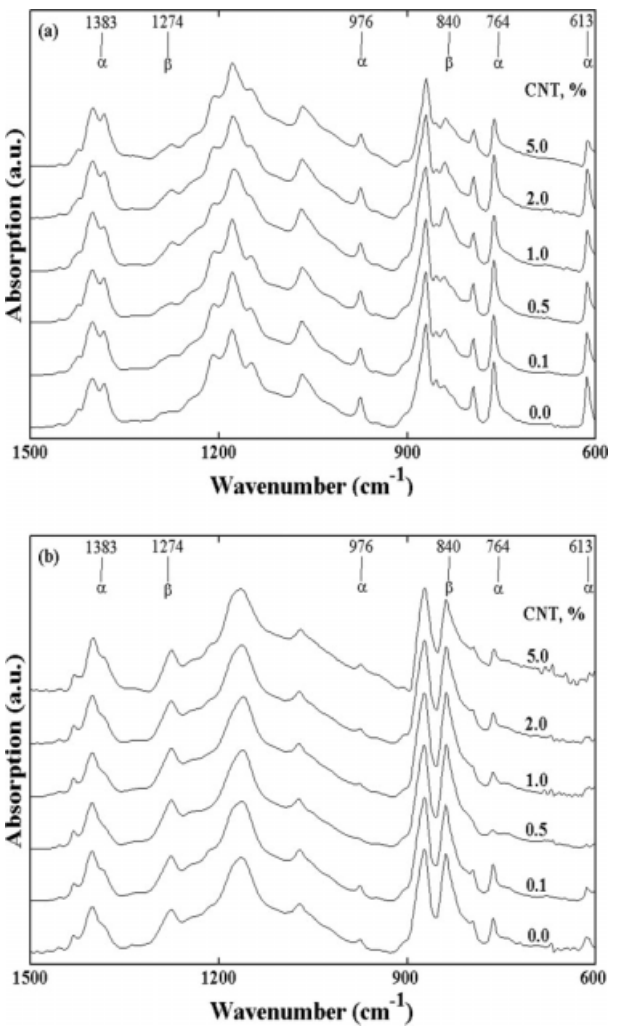

Figure 6 Normalized infrared absorption versus wavenumber for nanocomposites of PVDF with MWCNT. (a) Unoriented samples, (b) Oriented zone drawn samples. Absorption bands for alpha and beta PVDF are marked.

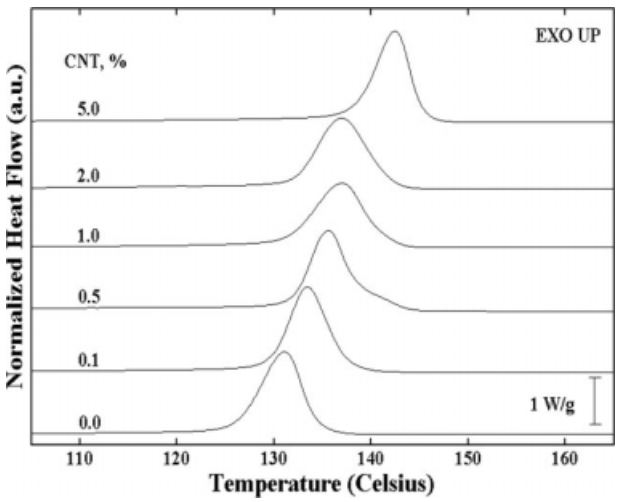

Figure 7 Normalized heat flow versus temperature for nanocomposites of PVDF with MWCNT during DSC cooling from 200°C at 10°C/min. The heat flow is normalized for PVDF sample mass. The exothermal peaks represent the crystallization peaks, at temperature T_c.

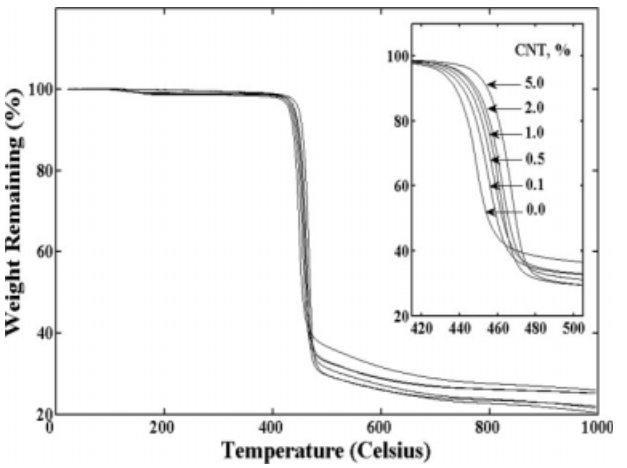

Figure 8 Thermogravimetic curve of weight remaining versus temperature for nanocomposites of PVDF with MWCNT. The insert plot of weight loss versus temperature is a magnification of the region between 400°C and 500°C.

Thermogravimetic analysis of unoriented sample films is shown in Figure 8. A major weight loss occurred in the region between 400 and 470°C for all samples. This is related to the degradation of PVDF and also to oxidization of MWCNT at around 450°C.[33] As can be seen, when the wt % of MWCNT increases, to obtain the same weight loss, higher temperature is needed for PVDF/MWCNT films in this region, which is shown in the insert plot of Figure 8 as a systematic shift of the thermogravimetic curve. The thermal stability of PVDF/MWCNT films was improved with MWCNT loading, a trend similar to what was observed by Liu's group.[34] A small weight loss, about 1% from 100°C to 170°C was also observed. This can be attributed to the evaporation of absorbed moisture and DMAc residue.

Residual weight percent remaining at different temperatures for PVDF/MWCNT is summarized in Table II. In Table II column 6, the weight percent remaining after major degradation at 500 to 1000°C was higher for PVDF than for PVDF/MWCNT films. This indicates MWCNT accelerates the degradation of PVDF at high temperature, above 500°C. One reason for this acceleration is that the HF monomer and a small amount of $C_4H_3F_3$ formed as a degradation product of PVDF[35] acted with MWCNT or its residue and caused a further degradation of the residual portion of the nanocomposites.

Mechanical properties

For unoriented films, the storage modulus increases with an increase in MWCNT concentration, and the glass transition is unaffected by adding MWCNT into the polymer matrix. This was observed by Liu's group as well, even though they used a different sample preparation method.[34] Figure 9(a) shows the

TABLE I
Thermal Parameters for Nanocomposites of PVDF with MWCNT

Sample (MWCNT wt %)[a]	T_c °C, (±0.5)[b]	T_c °C, (±0.5)[c]	T_c °C, (±2)[d]	ΔH_f J/g, (±1.5)[e]	χ_c (±1)[f]	ϕ_{ci} (±1)[g]
0.0	131.0	140.7	144	46.2	44	44
0.1	133.4	143.9	147	48.5	46	47
0.5	135.6	144.9	145	47.0	45	46
1.0	136.7	146.2	146	48.1	46	44
2.0	138.6	147.5	152	51.0	49	47
5.0	142.5	148.3	153	50.1	48	48

[a] PVDF/MWCNT unoriented film.
[b] Crystallization peak temperature from DSC at cooling rate of 10°C/min.
[c] Crystallization onset temperature from DSC at cooling rate of 10°C/min.
[d] Crystallization onset temperature from POM at cooling rate of 10°C/min.
[e] Heat of fusion from DSC at heating rate of 10°C/min.
[f] Degree of crystallinity calculated by eq. (2).
[g] Crystallinity index from 2D WAXS.

TABLE II
Thermogravimetric Results for Weight Remaining at Different Temperatures for PVDF/MWCNT Nanocomposites

	Weight remaining, % (±0.5)				
Sample (wt %)	400°C	450°C	500°C	600°C	1000°C
0.0	99.3	65.8	38.0	33.0	27.7
0.1	99.7	81.3	34.1	29.9	26.4
0.5	99.9	84.5	34.0	30.0	26.1
1.0	99.6	87.7	30.5	27.0	22.9
2.0	99.4	89.5	32.2	28.1	22.5
5.0	99.4	94.6	30.0	26.4	20.8

storage modulus, E', versus temperature for all unoriented samples. Because MWCNTs have a higher Young's modulus, by bonding to MWCNT, PVDF becomes stiffer (higher E'). This is further evidence that hydrogen bonds exist between MWCNT and PVDF.[13,36]

For oriented films, E' measured along the drawing direction is larger, as compared to unoriented films. Figure 9(b) shows a comparison of E's for unoriented and oriented samples at different frequencies, exemplified by 0.5 wt %. The mechanical response of PVDF nanocomposite to the oscillating strain along the drawing direction is smaller for oriented samples and causes a higher E'. This result shows that the zone drawing process rotates the gauche bond to trans bond whose energy is relatively lower, causing a permanent change of dipole in PVDF/MWCNT nanocomposites, and aligning the polymer chain in the drawing direction.

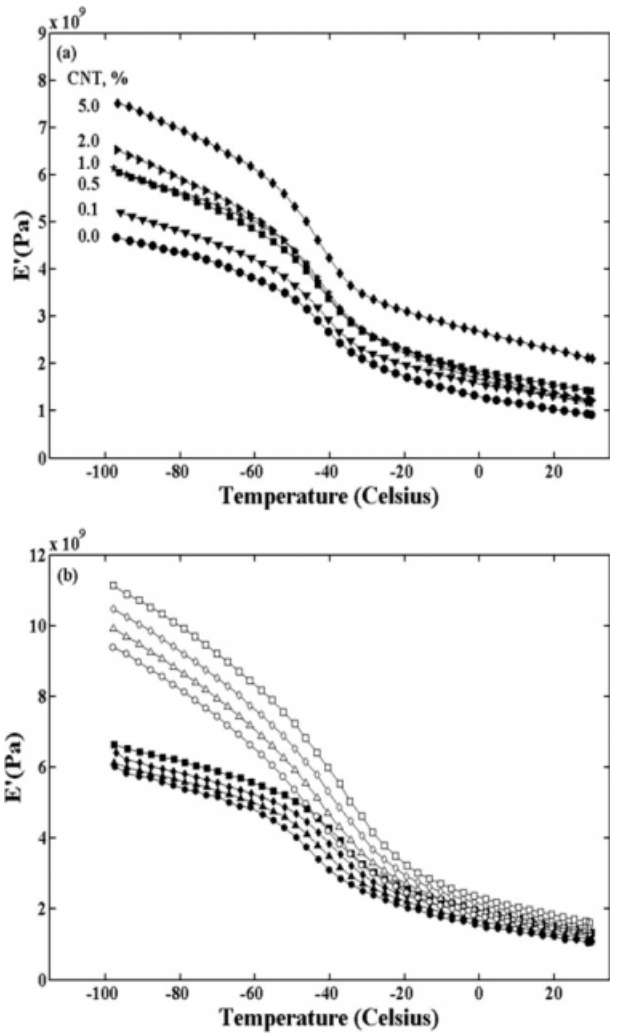

Figure 9 Storage modulus, E', versus temperature for nanocomposites of PVDF with MWCNT. (a) Unoriented sample for compositions as noted, (b) Unoriented samples (solid symbols) and oriented zone drawn samples (unfilled symbols) at different frequencies: 0.1 Hz (circle), 1.0 Hz (triangle), 10 Hz (diamond) and 50 Hz (square), exemplified by 0.5 wt %.

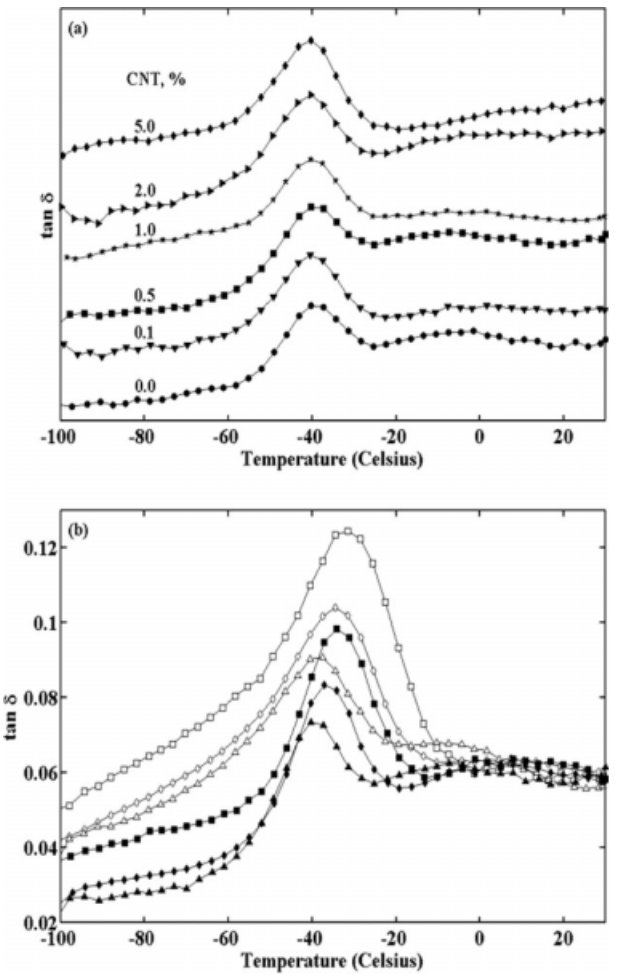

Figure 10 Loss factor, tan δ, versus temperature for nanocomposites of PVDF with MWCNT. (a) Unoriented sample for compositions as noted; curves have been displaced vertically for clarity, (b) Unoriented samples (solid symbols) and oriented zone drawn samples (unfilled symbols) at different frequencies, 1.0 Hz (triangle), 10 Hz (diamond) and 50 Hz (square), exemplified by 0.5 wt %.

TABLE III
Tan δ Peak Temperature at Different Frequencies for PVDF/MWCNT Nanocomposites

	Temperature (°C)						
	Unoriented (±0.5)			Oriented (±0.5)			
Sample (wt %)	1.0 Hz	10 Hz	50 Hz	0.1 Hz	1.0 Hz	10 Hz	50 Hz
0.0	−39.9	−36.1	−32.6	−40.5	−37.0	−33.6	−31.3
0.1	−40.5	−37.1	−34.5	−40.5	−37.1	−34.3	−31.1
0.5	−39.9	−37.1	−34.3	−40.7	−37.7	−34.3	−31.4
1.0	−40.5	−37.5	−34.1	−41.9	−37.5	−34.3	−31.5
2.0	−40.3	−37.1	−34.3	−40.3	−36.9	−31.2	−29.6
5.0	−40.3	−37.3	−34.3	−43.5	−37.5	−34.5	−31.3

The dielectric relaxation that occurred in PVDF/MWCNT[37] has also been studied by DMA. The loss factor, tan δ, can be obtained by:

$$\tan \delta = E''/E' \quad (3)$$

where E' is the storage modulus related to the elastic deformation, and E'' is the loss modulus related to the viscous deformation and energy absorption.[38]

The peak position of tan δ is assigned to glass transition, the segmental motions of polymer chain in the amorphous regions, and usually labeled as the β-transition.[39] Glass transition is a quasi-second order phase transition involving no latent heat. Above the glass transition temperature, T_g, there is sufficient mobility inside the polymer matrix, so that large scale reorganization of polymer chains can occur in response to an applied mechanical force. Below T_g the chains are frozen in position, and only small scale vibrational motion is possible. Figure 10(a) compares the tan δ peak position for all compositions for unoriented samples, and Figure 10(b) compares the tan δ peak for unoriented samples and oriented samples at different frequencies, exemplified by 0.5 wt %. A major relaxation was observed between −60°C and −10°C. The peak position of tan δ, referring to T_g, is independent of the concentration of MWCNT in both cases we studied, as shown in Figure 10(a). A slight shift of T_g, about 3°C, to a higher temperature from unoriented sample to oriented sample is observed, as shown in Table III. For oriented sample, the volume of amorphous region is larger, but it is more confined by aligned polymer chains ($\lambda \sim 4.7$) and MWCNT, thus a higher temperature is needed for the relaxation. We also observe that T_g increases with the frequency, which shows a phase delay in mechanical response of films at a higher frequency.

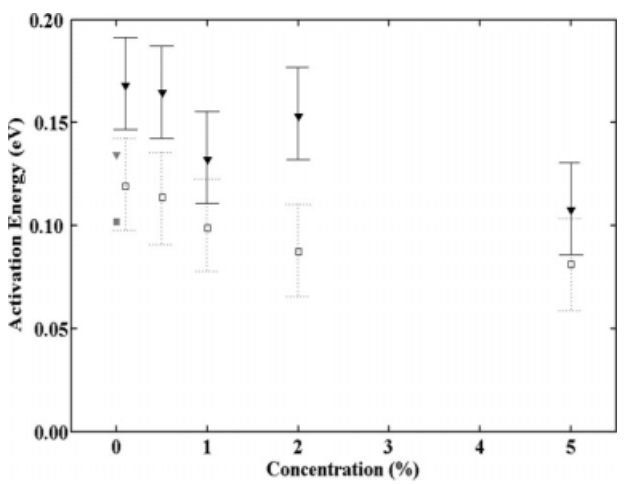

Figure 11 Activation energy versus concentration for unoriented (solid triangles) and oriented (empty squares) nanocomposites of PVDF with MWCNT. Pure PVDF is marked in gray for reference.

The relaxation time for the β-transition follows Vogel-Fulcher-Tamman-Hesse (VFTH) equation.[40,41]

$$\tau = \tau_0 \exp[B/k(T - T_0)] \quad (4)$$

where τ is the relaxation time for β-transition, $k = 1.38 \times 10^{-23}$ JK^{-1} is Boltzmann's constant, T_0 is the Vogel temperature ($T_0 = 170$ K for PVDF[40]), which is usually 30–70 K below T_g, and B is a constant activation energy. Molecules must acquire an extra amount of energy to pass the energy barrier from state a to state b.

The activation energy for unoriented PVDF and oriented PVDF has been estimated using both DSC and DMA data. DSC heating rate was transformed to an equivalent frequency.[42,43] By fitting logarithm frequency from DSC and DMA with reciprocal glass transition temperature (determined by tan δ peak position in DMA), we obtained best fit lines in an Arrhenius plot (not shown in the interest of brevity). The slope of the best fit lines is the activation energy. Figure 11 depicts the estimated activation energy from Arrhenius plots versus MWCNT concentration. The activation energy is in the range of 0.08–0.17 eV.

Mechanical properties were also evaluated by tensile testing at room temperature. The modulus of

TABLE IV
Mechanical Properties from Tensile Testing at Room Temperature for PVDF/MWCNT Nanocomposites, at Various Crosshead Speeds[a]

Sample (wt %)	Young's Modulus, GPa, (±0.05)		Proportional limit, MPa, (±0.5)		UTS (ultimate tensile stress), MPa (±0.5)		Strain at UTS, % (±1.0)	
	2	10	2	10	2	10	2	10
0.0	1.46	1.25	7.0	9.1	4.2	4.3	8.5	9.6
0.1	1.46	1.47	8.5	11.4	4.4	4.7	8.1	8.0
0.5	1.52	1.48	9.7	13.0	4.5	4.6	7.3	7.6
1.0	1.61	1.58	10.2	12.1	4.5	4.7	7.3	7.6
2.0	1.70	1.52	11.7	12.2	4.4	4.7	6.7	6.7
5.0	1.82	1.76	11.9	11.0	4.5	4.6	5.5	6.4

[a] Crosshead speeds of 2 or 10 mm/min.

elasticity (Young's modulus) was calculated using least squares fitting within the low strain (linear) portion of stress–strain curve, which follows Hooke's law:

$$\sigma_e = E\ \varepsilon_e \tag{5}$$

where σ_e is the stress applied, ε_e is the strain, and E is Young's modulus of the sample. The proportional limit was determined by offsetting a line parallel to the tangency line by 0.02% strain. The intersection of the offset line and the stress–strain curve is used to estimate the proportional limit.[44] The ultimate tensile strength (UTS) was determined by the highest stress value over the entire stress–strain curve from elongation until failure. In Table IV, as expected, the nanocomposites with the greater weight percent of MWCNT have greater Young's moduli and greater proportional limits. The nanocomposite with highest weight percent of MWCNT, 5 wt %, has the highest average Young's modulus and UTS of 1.82 ± 0.05GPa and 44.7 ± 0.5MPa, respectively, at a crosshead speed of 2 mm/min. The average Young's modulus and UTS of pure PVDF are 1.46 ± 0.05 GPa and 42.0 ± 0.5 MPa, respectively. The strain at UTS decreases as weight percentage of MWCNT increases. Typical stress–strain curves at 2 mm/min for all nanocomposites in the low strain region are shown in Figure 12. The tests with crosshead speed of 10 mm/min (not shown for the sake of brevity) presented a similar graph. This result shows that the high weight percent nanocomposite is stiffer than pure PVDF. By adding nanofiller with large Young's modulus, the mechanical properties of the polymer nanocomposite were also improved.

CONCLUSIONS

Nanocomposites of poly(vinylidene fluoride) (PVDF) with mutiwalled carbon nanotubes (MWCNTs) have been investigated over a wide composition range, from 0.1 to 5.0% MWCNT by weight. The effect of zone drawing on these nanocomposites is also studied by comparing the oriented samples with unoriented samples. The conclusions are summarized as follows:

1. MWCNTs have negligible effect on forming beta crystal in PVDF (inducing only a tiny portion of beta phase crystal (1–2%) in the PVDF/MWCNT films). Zone drawing causes a significant alpha to beta transition in PVDF/MWCNT strips. In this process the beta phase grew at the expense of alpha phase, but the total degree of crystallinity decreased.
2. MWCNT acts as nucleation agent during crystallization and slightly increases the degree of crystallinity of both unoriented and oriented PVDF/MWCNT films. Crystallization temperature, T_c, for PVDF/MWCNT films increases with MWCNT concentration.

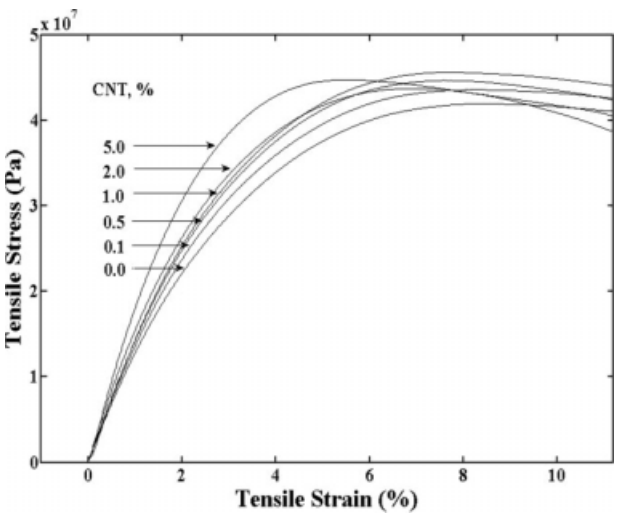

Figure 12 Stress–strain curves at room temperature in the low strain region at a cross head speed of 2 mm/min for nanocomposites of PVDF with MWCNT.

3. The lower temperature thermal stability for PVDF/MWCNT is also improved (nanocomposites show a higher degradation temperature below 500°C) when MWCNT concentration increases.
4. The glass transition temperature, T_g, measured by the peak position of tan δ does not change with MWCNT concentration, but a higher T_g can be obtain by zone drawing.
5. Dynamic storage modulus, E', was improved when MWCNT concentration increases in unoriented PVDF/MWCNT film. Zone drawing also generally increases E'.
6. Young's modulus and the proportional limit from stress–strain curves increase, while strain at the point of ultimate tensile stress decreases, as MWCNT concentration increases.

Undergraduate summer interns K. Edenzon, L. Fernandez, S. Razmpour, and J. Woodburn performed the research at Tufts University. The author thanks Mr. J. Kluge for the help with mechanical test experiments, Dr. H. Chen for the help with SEM work, and Prof. Georgi Georgiev (Assumption College) for purification of the MWCNTs.

References

1. Lang, S. B.; Muensit, S. Appl Phys A: Mater Sci Process 2006, 85, 125.
2. Lovinger, A. J. Science 1983, 220, 1115.
3. Nakagawa, K.; Ishida, Y. Kolloid-Zeitschrift and Zeitschrift Fur Polymere 1973, 251, 103.
4. Kawai, H. Jpn J Appl Phys 1969, 8, 975.
5. Bergman, J. G.; Mcfee, J. H.; Crane, G. R. Appl Phys Lett 1971, 18, 203.
6. Branciforti, M. C.; Sencadas, V.; Lanceros-Mendez, S.; Gregorio, R. J Polym Sci Part B: Polym Phys 2007, 45, 2793.
7. Gregorio, R.; Cestari, M. J Polym Sci Part B: Polym Phys 1994, 32, 859.
8. Priya, L.; Jog, J. P. J Polym Sci Part B: Polym Phys 2003, 41, 31.
9. Buckley, J.; Cebe, P.; Cherdack, D.; Crawford, J.; Ince, B. S.; Jenkins, M.; Pan, J. J.; Reveley, M.; Washington, N.; Wolchover, N. Polymer 2006, 47, 2411.
10. Iijima, S. Nature 1991, 354, 56.
11. Safadi, B.; Andrews, R.; Grulke, E. A. J Appl Polym Sci 2002, 84, 2660.
12. Levi, N.; Czerw, R.; Xing, S. Y.; Iyer, P.; Carroll, D. L. Nano Lett 2004, 4, 1267.
13. Jin, Z. X.; Pramoda, K. P.; Goh, S. H.; Xu, G. Q. Mater Res Bull 2002, 37, 271.
14. Rangari, V. K.; Yousuf, M.; Jeelani, S.; Pulikkathara, M. X.; Khabashesku, V. N. Nanotechnology 2008, 19, 9.
15. Bikiaris, D.; Vassiliou, A.; Chrissafis, K.; Paraskevopoulos, K. M.; Jannakoudakis, A.; Docoslis, A. Polym Degrad Stab 2008, 93, 952.
16. Tu, Z. C.; Ou-Yang, Z. Phys Rev B 2002, 65, 4.
17. Treacy, M. M. J.; Ebbesen, T. W.; Gibson, J. M. Nature 1996, 381, 678.
18. Tang, W. Z.; Santare, M. H.; Advani, S. G. Carbon 2003, 41, 2779.
19. Kim, P.; Shi, L.; Majumdar, A.; Mceuen, P. L. Phys Rev Lett 2001, 87, 4.
20. Wang, M.; Shi, J. H.; Pramoda, K. P.; Goh, S. H. Nanotechnology 2007, 18, 7.
21. Chen, H.; Liu, Z.; Cebe, P. Polymer 2009, 50, 872.
22. Aihara, Y.; Cebe, P. Polym Eng Sci 1994, 34, 1275.
23. Berns, D. M.; Oyebode, E.; Dair, B.; Cebe, P.; Capel, M. J Appl Polym Sci 2001, 82, 3492.
24. Bachmann, M. A.; Lando, J. B. Macromolecules 1981, 14, 40.
25. Matsushige, K.; Nagata, K.; Imada, S.; Takemura, T. Polymer 1980, 21, 1391.
26. Gutierrez, M. C. G.; Alfonso, G. C.; Riekel, C.; Azzurri, F. Macromolecules 2004, 37, 478.
27. Freimuth, H.; Sinn, C.; Dettenmaier, M. Polymer 1996, 37, 831.
28. Yang, Z. L.; Chen, H. Z.; Cao, L.; Li, H. Y.; Wang, M. Mater Sci Eng B: Solid State Mater Adv Technol 2004, 106, 73.
29. Wang, Y. H.; Li, Y. N.; Lu, J.; Zang, J. B.; Huang, H. Nanotechnology 2006, 17, 3817.
30. Kobayashi, M.; Tashiro, K.; Tadokoro, H. Macromolecules 1975, 8, 158.
31. Crabtree, R. H.; Eisenstein, O.; Sini, G.; Peris, E. Meeting of the Groupe-d-Etude-en-Chimie-Organometallique/Concertation-en-Chimie-de-Coordination (GECOM-CONCOORD 97), France. May 19–23 1997, p 7.
32. Minh, N. Q. J Am Ceram Soc 1993, 76, 563.
33. Hou, P. X.; Bai, S.; Yang, Q. H.; Liu, C.; Cheng, H. M. Carbon 2002, 40, 81.
34. Chen, D.; Wang, M.; Zhang, W. D.; Liu, T. X. J Appl Polym Sci 2009, 113, 644.
35. Zulfiqar, S.; Zulfiqar, M.; Rizvi, M.; Munir, A.; Mcneill, I. C. Polym Degrad Stab 1994, 43, 423.
36. Tran, M. Q.; Shaffer, M. S. P.; Bismarck, A. Macromol Mater Eng 2008, 293, 188.
37. Singh, R.; Kumar, J.; Singh, R. K.; Kaur, A.; Sinha, R. D. P.; Gupta, N. P. Polymer 2006, 47, 5919.
38. Sencadas, V.; Lanceros-Mendez, S.; Mano, J. F. Thermochim Acta 2004, 424, 201.
39. Liu, Z. H.; Marechal, P.; Jerome, R. Polymer 1997, 38, 4925.
40. Ozkazanc, E.; Guney, H. Y.; Oskay, T.; Tarcan, E. J Appl Polym Sci 2008, 109, 3878.
41. Mijovic, J.; Ristic, S.; Kenny, J. Macromolecules 2007, 40, 5212.
42. Huo, P. P. T.; Cebe, P. Symposium on Advances in Polymer Matrix-Based Composites, Presented at the Meeting of the American Chemical Society, San Francisco, CA, April 1992, pp 696.
43. Hensel, A.; Dobbertin, J.; Schawe, J. E. K.; Boller, A.; Schick, C. J Therm Anal 1996, 46, 935.
44. Davis, J. R. Tensile Testing; 2nd ed.; ASM International: Materials Park, Ohio; 2004; 270–272.